Research Square

Preprints are preliminary reports that have not undergone peer review.
They should not be considered conclusive, used to inform clinical practice,
or referenced by the media as validated information.

Oral strontium chloride alleviates ovariectomy-induced bone loss in rats by remodeling the gut microbiota

[redacted]
Chinese Academy of Agricultural Sciences
[redacted]
Chinese Academy of Agricultural Sciences
[redacted]
Chinese Academy of Agricultural Sciences
[redacted]
Chinese Academy of Agricultural Sciences
[redacted]
Chinese Academy of Agricultural Sciences
[redacted]
zhengnan@caas.com

Chinese Academy of Agricultural Sciences

Research Article

Keywords: Strontium, Postmenopausal osteoporosis, Bone micro-structure, metabolism, Microbiota–metabolite–bone axis

Posted Date: November 18th, 2026

DOI: https://doi.org/10.21203/rs.3.rs-11604098/v1

License: This work is licensed under a Creative Commons Attribution 4.0 International License.
Read Full License

Additional Declarations: No competing interests reported.

Abstract

Background

Postmenopausal osteoporosis (PMOP) is a common skeletal disorder caused by estrogen loss, which shifts bone remodeling toward resorption. Sr is a bone-seeking trace element with established effects on bone turnover and microarchitecture, but its relationship with gut microbial and fecal metabolic changes in PMOP is not well defined.

Objective

We asked whether oral $SrCl_2$ reduces OVX-induced bone loss and whether any skeletal benefit coincides with gut microbiota and fecal metabolite changes.

Methods

Female Sprague–Dawley rats were sham-operated or ovariectomized (OVX). OVX animals received vehicle or $SrCl_2 \cdot 6H_2O$ (200 mg/kg/day) for 42 days (n = 6 per group). We measured serum turnover markers and cytokines, femoral biomechanics, trabecular microarchitecture and histomorphometry, and profiled the fecal microbiota (16S rRNA sequencing) and metabolome (untargeted LC-MS). MC3T3-E1 osteoblasts challenged with dexamethasone were used to test direct effects of Sr.

Results

OVX raised bone turnover and IL-6 and reduced biomechanical and trabecular parameters; Sr reversed these changes. Sr also shifted the microbiota (higher Romboutsia and Turicibacter, lower Streptococcus and Lachnospiraceae) and the fecal lipid profile, including the oxylipins (±)11(12)-EET, 9(S)-HOTrE and 13(S)-HOTrE and PC(18:2/20:3). Fecal (±)11(12)-EET correlated with bone turnover, microarchitecture and biomechanics. In DEX-treated MC3T3-E1 cells, Sr increased proliferation, osteogenic markers and mineralization.

Conclusions

Oral $SrCl_2$ protects against OVX-induced bone loss and promotes osteoblast differentiation and mineralization. The accompanying gut microbiota and fecal oxylipin changes suggest a microbiota–oxylipin–bone axis that warrants further testing; Sr-enriched foods may offer a route to support postmenopausal bone health.

Highlights

1 Dietary strontium chloride reduces ovariectomy-induced bone loss without harming visceral organs in rats.

2 Dietary strontium reshapes the gut microbiota and improves intestinal homeostasis in ovariectomized rats.

3 Strontium alters linoleic acid metabolism, and the lipid (±)11(12)-EET tracks multiple bone phenotypes.

4 In cultured pre-osteoblasts, strontium reverses dexamethasone-induced loss of proliferation and mineralization.

1. Introduction

As the population ages, postmenopausal osteoporosis (PMOP) has increasingly emerged as a significant concern due to its high incidence and disability rate [1–3]. The random-effects model revealed that about 36% of Chinese people aged 60 and older had osteoporosis (OP) on average, with 23% attributed to men and 49% to women [4]. This divergence primarily stems from the decrease in ovarian function occurring in women after menopause, consequently precipitating PMOP [5]. The negative balance between osteoblasts and osteoclasts during bone remodeling is the main pathogenesis of PMOP [6]. Lately, researchers have discovered a close correlation between the onset of PMOP and both inflammatory responses and gut microbiota dysbiosis [7].

The gut microbiota is the body's largest microbial community and contributes to bone metabolism [8–12]. Ovariectomy (OVX) failed to cause the usual bone loss in germ-free mice, implying that the microbiota are needed for estrogen-deficiency bone loss [13, 14]. Microbial signals also modulate inflammatory pathways linked to PMOP [7, 15]. In OVX mice, loss of sex steroids raised intestinal and bone-marrow TNF-α, RANKL and IL-17 [14], whereas probiotics reduced trabecular bone loss by dampening this inflammation. Microbial metabolites can further influence the balance between bone formation and resorption. In OVX mice, 16S rDNA sequencing and UHPLC-MS showed that a drug intervention restored gut homeostasis, decreased Helicobacter and trimethylamine N-oxide (TMAO)-related metabolites, and limited estrogen-deficiency bone loss [13]. These observations support the “microbiota–metabolite–bone” axis as a framework for PMOP.

Sr occurs widely in soil, water, food and air, and people are exposed mainly through diet and drinking water [16]. Once absorbed, Sr is deposited preferentially in bone. About 99% of the body burden resides in bone, where it replaces calcium in hydroxyapatite and affects bone remodeling [16, 17]. Sr taken up from water is roughly twice that from solid food, and high calcium intake or alginates can further limit uptake [17]. Ranelate, citrate and chloride salts of Sr have all been tested as dietary supplements in ovariectomized models [18]. Sr is also well known for bone-protective activity. It promotes osteoblast differentiation and suppresses osteoclast formation and resorption [19, 20]. Strontium ranelate has been approved for clinical use in osteoporosis [21–24]. Because Sr occurs naturally in food and water, it is an attractive trace element for nutritional strategies aimed at bone health.

Sr is well known for improving bone mass. Whether its benefits in PMOP are accompanied by coordinated changes in the gut microbiota and fecal metabolome, and whether such changes relate to skeletal outcomes, remains poorly defined. In this study, OVX rats received dietary $SrCl_2$; we measured bone turnover markers, femoral biomechanics, microarchitecture and histomorphometry, profiled the fecal microbiota and metabolome, and tested the direct effects of Sr on osteoblasts in vitro. The resulting dataset provides an exploratory, multi-level description of Sr action in a female PMOP model and generates hypotheses on how Sr, gut microbial ecology and host lipid metabolism may interact.

2. Materials and methods

2.1 Chemicals and reagents

$SrCl_2 \cdot 6H_2O$ (AKSL-051059) was obtained from Beijing Aikesailun Co., Ltd. ELISA kits for P1NP (YX-E171416-48T), ALP (YX-E011216), TRACP (YX-E201919), CTX (YX-E23024), E2 (YX-E050200), IL-6 (YX-E091206), PTH (YX-E162008) and VD3 (YX-E220403) were supplied by Shanghai Yuanxin Co., Ltd. The HiPure Stool DNA kit came from Guangzhou Magen Co., Ltd.

2.2 Animals and treatments

Female Sprague–Dawley rats (12 weeks old, specific-pathogen-free) were purchased from Beijing Vital River Laboratory Animal Technology Co., Ltd. (Beijing, China). The animals were kept at 22 ± 3°C and 45–60% humidity with a 12-h light/dark cycle. Food and water were provided ad libitum, and the rats were acclimatized for 7 days before the study. Using a random number table and body-weight stratification, we allocated the rats to Sham, OVX and OVX-Sr groups (n = 6 per group). Body weight was measured every 3 days.

The Committee on the Ethics of Animal Experiments of the Chinese Academy of Agricultural Sciences approved the study (IAS2022-146), which followed institutional guidelines. The study was not prospectively registered.

At the end of the study, feces were collected after the last gavage and stored at − 80°C for microbiome analysis. After a 12-h fast, rats were euthanized with an overdose of pentobarbital sodium (150 mg/kg, i.p.), and blood and organs were collected. Uterus, spleen, kidney, stomach, heart and liver were photographed and weighed. Left femurs were kept at − 20°C for micro-CT and histology, right femurs at 4°C for mechanical testing, and serum at − 20°C for ELISA.

2.3 OVX model establishment

Bilateral ovariectomy (OVX) or Sham surgery was carried out in 12-week-old female SD rats under sodium pentobarbital anesthesia (40–50 mg/kg, i.p.). A dorsal midline incision was made; the ovarian pedicle was ligated with sterile absorbable suture, and both ovaries were removed. Sham rats received the same incision with removal of a small amount of periovarian fat. The incision was closed in layers. Carprofen (5 mg/kg, s.c.) was used for postoperative analgesia. Rats were kept warm during surgery and

checked until recovery, then monitored daily for 3 days and at least every 3 days thereafter. Successful OVX was confirmed by lower uterine weight and serum E2 in OVX rats than in Sham rats (Figure S1B, C). The rats were assigned to three groups (n = 6 per group): Sham (purified water), OVX (purified water) and OVX-Sr ($SrCl_2 \cdot 6H_2O$, 200 mg/kg BW). Water or $SrCl_2 \cdot 6H_2O$ was given by gavage once daily for 42 days. Six rats per group were used, consistent with our earlier study, previous OVX rat studies and the 3R principles. Rats that died, developed severe postoperative complications, or lost > 20% of body weight were excluded; none were excluded. Humane endpoints were > 20% body-weight loss, inability to access food or water, a moribund state, or severe surgical complications; affected rats would have been euthanized at once.

2.4 Serum biochemical parameter testing

Serum Sr^{2+} was determined by ICP-MS (Agilent 7700). Ca^{2+} and phosphorus were measured with an automated biochemistry analyzer (Rayto, Chemray 800). Serum P1NP, ALP, TRACP, CTX, PTH, VD3 and IL-6 were quantified by ELISA according to the manufacturer's instructions.

2.5 Bone mechanical testing

Each femur was mounted in a texture analyzer (TAXT Plus, Stable Micro Systems) and loaded at 24 mm/min. Elastic modulus (N/mm), maximum load (N) and breaking deformation (mm) were recorded.

2.6 Micro-CT analysis

Femurs were imaged with micro-CT (SkyScan 1275, Bruker) at 9 μm resolution. Images were reconstructed with NRecon (v1.7.4.2), and CT Analyzer v1.20.3.0 was used to analyze 400 cross-sections of the distal femur. The parameters measured were BS/BV (1/mm), Tb.Pf (1/mm), Tb.Th (mm) and BMD (g/cm^3).

2.7 H&E staining

Femurs were decalcified in EDTA, embedded and sectioned. Sections were stained with H&E; nuclei were blue and cytoplasm red.

2.8 Goldner's trichrome staining

Samples were processed as in Section 2.7 and stained with trichrome solution. Mineralized bone appeared green, non-mineralized bone orange-red, and nuclei purple-black or gray-black.

2.9 TRAP staining

Samples were processed as in Section 2.7 and incubated with TRAP solution for 20 min. Cells with ≥ 3 nuclei and positive staining were counted as TRAP-positive osteoclasts.

2.10 Gut microbiota sequencing analysis

Six fecal samples per group were used for DNA extraction and purification with the HiPure Stool DNA kit. After confirming nucleic acid purity and integrity, the V3–V4 region of the 16S rRNA gene was amplified

with primers 341F (5′-CCTACGGGNGGCWGCAG-3′) and 806R (5′-GGACTACHVGGGTATCTAAT-3′). Sequencing was performed on an Illumina HiSeq instrument. QIIME 1.9.1, Vegan 2.5.3, ggplot2 2.2.1 and LEfSe 1.0 were used for bioinformatics analysis.

2.11 Metabolomics analysis

Untargeted metabolomics used a Dionex Ultimate 3000 chromatograph coupled to a Q Exactive mass spectrometer and a Thermo Syncronis C18 column (100 mm × 2.1 mm, 1.7 μm). Feces were extracted with 80% methanol and centrifuged at 15,000 × g for 20 min at 4°C. The supernatant was diluted to 53% methanol and centrifuged again, and the final supernatant was analyzed by LC-MS. Mobile phase A was water with 0.1% formic acid and 2 mmol/L ammonium formate; mobile phase B was acetonitrile. The gradient was 0–1 min, 95% A; 1–5 min, 95–40% A; 5–8 min, 40–0% A; 8–11 min, 0% A; 11–14 min, 0–40% A; 14–15 min, 40–95% A; 15–18 min, 95% A. Electrospray ionization was set at 2.8 kV with sheath and auxiliary gas flows of 35 and 10 arb, and the capillary temperature was 320°C. Samples were run in positive and negative modes. Six pooled QC samples were used to monitor stability. Candidate differential metabolites were selected by VIP > 1 and $P < 0.05$, with additional fold-change and ROC filtering, and the resulting lists are reported in the Results.

2.12 Cell assays

1. Cell culture and treatments

MC3T3-E1 mouse embryonic osteoblasts were purchased from the American Type Culture Collection (Manassas, VA, USA). Cells were maintained in medium with 1% antibiotics (100 units/mL penicillin and 100 μg/mL streptomycin) and 12% (v/v) FBS at 37°C and 5% CO_2, and were incubated for 2 days.

Dexamethasone (DEX) was used to injure osteoblasts in vitro, and $SrCl_2$ was tested as the intervention. Cells were exposed to DEX (0–5 μM) and $SrCl_2$ (0–128 μg/mL) for 2 days, then harvested for viability, biochemical and staining assays.

2. Cell viability assay

Cells received DEX (0, 0.01, 0.5, 1, 5 μM) alone or with $SrCl_2$ (0, 16, 32, 64, 128 μg/mL) for 48 h. CCK-8 reagent was added for 4 h, and absorbance was read at 570 nm (Thermo Company, Waltham, MA, USA).

3. Osteogenesis-related markers detection

After treatment, medium was removed, cells were washed twice with PBS, and samples were fixed in 4% paraformaldehyde. ELISA was used to measure ALP, BMP-2, BSP, CBF-α1, CT, OCN, P1NP and RUNX2 (standard curves in Figure S4).

4. ALP and ARS staining

Samples were processed as in Section 2.12. ALP and ARS staining was performed 7 and 14 days after osteogenic induction. ALP activity was detected with an ALP kit (Solarbio), and mineralized nodules were visualized with an ARS kit (Solarbio); stained cells were viewed under a light microscope (Olympus).

5. RUNX2 Immunofluorescence staining

Samples were processed as in Section 2.12. Cells were permeabilized with 0.2% Triton X-100 and incubated overnight with a RUNX2 primary antibody, followed by a 30-min incubation with a fluorescent secondary antibody in the dark. Nuclei were stained with DAPI, and RUNX2-positive puncta were examined by confocal microscopy.

2.13 Statistical analysis

GraphPad Prism 6.0 was used for statistics. Multiple-group comparisons used one-way ANOVA with Tukey's post hoc test. Pearson correlation and linear regression were used to assess relationships. Data are shown as mean ± SD, with replicate numbers in the figure legends. *, $P < 0.05$. **, $P < 0.01$. ***, $P < 0.001$ vs. Sham/CTL. #, $P < 0.05$. ##, $P < 0.01$. ###, $P < 0.001$ vs. OVX/DEX. The primary outcomes were serum P1NP and micro-CT Tb.Th; other parameters were secondary or exploratory. Investigators were not blinded to group allocation.

3. Results

3.1 General physiological responses and organ safety of oral strontium supplementation in ovariectomized rats

Figure 1A outlines the experimental workflow, and Figure S1A shows the Sham procedure and ovary removal. Serum E2 was lower in OVX rats than in Sham rats ($P < 0.001$, Figure S1B), confirming successful ovariectomy and validating the model. Body weight was recorded every 3 days. After 42 days of Sr treatment, OVX and OVX + Sr rats weighed more than Sham rats ($P < 0.01$, Fig. 1B). Uterus weight was lower in OVX rats ($P < 0.001$, Figure S1C), whereas spleen, kidney, stomach, heart and liver weights were comparable among groups ($P > 0.05$, Figure S1D–H). Sr thus did not affect the mass or morphology of these organs.

3.2 Sr alleviated high bone turnover, inflammatory response and impaired femoral biomechanical properties in OVX rats

OVX rats had higher serum P1NP ($P < 0.001$), ALP ($P < 0.01$), TRACP ($P < 0.005$) and CTX ($P < 0.01$) than Sham rats, indicating accelerated bone turnover; Sr treatment blunted these increases (Fig. 2A–D). PTH

and vitamin D_3 followed similar patterns, consistent with reduced turnover and less bone loss after Sr ($P < 0.001$, Table S1). Serum IL-6 rose after OVX and fell with Sr ($P < 0.05$, Fig. 2E). Three-point bending tests showed lower maximum load, breaking deformation and energy to ultimate load in OVX rats; Sr restored these parameters ($P < 0.05$, Fig. 2F–H).

3.3 Sr attenuated OVX-induced deterioration of bone microstructure and morphology

Micro-CT showed thinner, sparser trabeculae in OVX rats than in Sham rats, indicating postsurgical bone loss. OVX-Sr rats had thicker, more regularly arranged trabeculae with smaller trabecular gaps and marrow cavities (Fig. 3A). BS/BV, Tb.Pf and Tb.Th differed between OVX and OVX-Sr rats ($P < 0.05$, Fig. 3B–D), whereas BMD did not ($P > 0.05$, Fig. 3E).

H&E and Goldner staining depicted femoral histomorphology (Fig. 3F). Goldner staining revealed higher Tb.Pm, Tb.Ar and Tb.Th in Sr-treated rats ($P < 0.05$, Fig. 3G–I), in line with micro-CT. TRAP staining showed more trabecular bone and fewer osteoclasts in the distal femur of OVX-Sr rats than in OVX rats (Fig. 3F).

3.4 Sr alleviated OVX-induced gut microbiota dysbiosis

OTU counts were 768, 769 and 718 in the Sham, OVX and OVX-Sr groups, with 518 OTUs shared by all groups (Fig. 4A and Table S2). The Sham and OVX-Sr communities were more similar to each other than to the OVX community, implying that Sr altered the intestinal microbiota (Fig. 4B). LEfSe with LDA scores identified taxa that differed among groups (Fig. 4C–D). Phylum- and genus-level compositions were similar in Sham and OVX-Sr rats (Fig. 4E–F and Data S1, S2). At the genus level, Romboutsia ($P < 0.01$), Turicibacter, Streptococcus and unidentified Lachnospiraceae ($P < 0.05$) differed between OVX and OVX-Sr rats (Fig. 4G–J). These taxa may contribute to the effects of Sr in PMOP.

3.5 Sr partially corrected the OVX-induced fecal metabolic disorder

PCA separated the metabolite profiles of the Sham, OVX and OVX-Sr groups (Fig. 5A; Data S3). Between Sham and OVX groups, 48 metabolites increased and 49 decreased (Fig. 5B; Data S4). In the OVX-Sr group, 31 metabolites were higher and 58 lower than in Sham rats (Fig. 5C; Data S5). Between OVX and OVX-Sr groups, 27 metabolites were higher in OVX rats and 9 were higher in OVX-Sr rats (Fig. 5D; Data S6).

Thirty-six metabolites differed between OVX and OVX-Sr rats. Enrichment analysis implicated linoleic acid metabolism, ether lipid metabolism and indole alkaloid biosynthesis (Fig. 5E and Data S6). Five metabolites were notable: (±)11(12)-EET (Fig. 5F), 9(S)-HOTrE (Fig. 5G), 13(S)-HOTrE (Fig. 5H), 1-O-hexadecyl-lyso-sn-glycero-3-phosphocholine (Fig. 5I) and PC(18:2/20:3) (Fig. 5J). OVX changed their abundances, and Sr reversed these changes.

3.6 Sr-responsive fecal metabolites are associated with bone turnover markers and bone phenotypes

Five Sr-responsive metabolites correlated with bone turnover markers (Fig. 6A). (±)11(12)-EET had the strongest associations and was chosen as the key metabolite. It was lower in Sr-treated rats and correlated with maximum load (R^2 = 0.3115, P = 0.0161), breaking deformation (R^2 = 0.4459, P = 0.0025), Tb.Th (R^2 = 0.3883, P = 0.0057), BS/BV (R^2 = 0.2416, P = 0.0383), P1NP (R^2 = 0.3805, P = 0.0064), ALP (R^2 = 0.3735, P = 0.007), CTX (R^2 = 0.2635, P = 0.0294) and TRACP (R^2 = 0.2478, P = 0.0355). These analyses used pooled data from all groups (n = 18) and are exploratory; causality was not tested. The pattern suggests that (±)11(12)-EET tracks the OVX-associated metabolic state (Fig. 6B–I) and may link Sr-responsive lipids to osteoblast function, which we tested in vitro (Fig. 7).

3.7 Sr directly rescues DEX-induced impairment of osteoblast proliferation and differentiation in vitro

We used a DEX-induced MC3T3-E1 injury model to test direct effects of Sr on osteoblasts (Fig. 7A) and examined proliferation, early differentiation and late mineralization. Viability fell most strongly at 1 μM DEX (Figure S3A-C). Combining 1 μM DEX with 0, 16, 32, 64 or 128 μg/mL Sr showed that 64 μg/mL Sr gave the best recovery of viability (P < 0.001, Figure S3B-C), so this concentration was used thereafter.

After 4 days, the osteogenic markers ALP, BMP-2, BSP, CBF-α1, CT, OCN, P1NP and RUNX2 were measured. Sr significantly reversed the DEX-induced decline in these markers (P < 0.01, Fig. 7B-I). At 7 and 14 days, microscopy showed that Sr opposed the effects of DEX, with more ALP-positive cells and greater calcium-nodule deposition. Immunofluorescence also showed higher cytosolic RUNX2 after Sr treatment (Fig. 7J).

4. Discussion

Sr is known to modulate bone homeostasis. Our earlier work showed that $SrCl_2$ improves bone mass in young male rats alongside gut microbiota changes [21]. Here we tested this in a PMOP model. In OVX rats, dietary $SrCl_2$ reduced high bone turnover, preserved femoral biomechanics and trabecular microarchitecture, and lowered osteoclast numbers. These changes coincided with gut microbiota and fecal metabolome remodeling, and several Sr-responsive metabolites, especially oxylipins, correlated with bone phenotypes. The results indicate that dietary $SrCl_2$ protects against OVX-induced bone loss and that this protection is closely linked to gut microbiota and fecal lipid/oxylipin changes. These data support a microbiota–metabolite–bone axis in the skeletal response to Sr, with (±)11(12)-EET as a candidate metabolite.

Sr lowered the OVX-induced rise in P1NP, ALP, TRACP and CTX and reduced circulating IL-6, consistent with less bone remodeling. Bone turnover markers are established indicators of remodeling [25] and are widely used to monitor treatment in postmenopausal osteoporosis. Femoral three-point bending and

trabecular indices improved after Sr treatment (BS/BV, Tb.Pf, Tb.Th, Tb.Pm and Tb.Ar), and TRAP staining showed fewer osteoclasts. The results agree with the dual action of Sr on bone cells, supporting osteoblasts and restraining osteoclasts [21–24], and with the direct pro-osteogenic effect seen in MC3T3-E1 cells (below). Serum Ca was slightly higher and serum P lower in OVX-Sr rats than in OVX rats, while PTH and vitamin D_3 approached Sham levels (Table S1), suggesting better calcium–phosphorus balance rather than simple suppression of remodeling. Trabecular microarchitecture, histomorphometry and biomechanics improved consistently. Distal-femur BMD did not change significantly, perhaps because this measure is relatively insensitive to mainly trabecular changes at this site.

Sr enters the body mainly through food and drinking water. Drinking-water Sr varies geographically (0.005–3.11 mg/L across Chinese cities; mean, 0.360 mg/L) [16, 26]. Sr is absorbed about twice as efficiently from water as from solid food [17], and it is deposited mainly in bone, where it replaces calcium in the mineral lattice and participates in remodeling [16, 17]. Sr-rich mineral water and Sr-containing foods are therefore plausible nutritional sources. In this study, oral $SrCl_2$ improved bone turnover, trabecular microarchitecture and biomechanics, alongside gut microbiota and fecal oxylipin changes. These results support the potential of Sr as a bone-protective trace element and warrant further work on Sr-containing foods and mineral waters.

OVX shifted the fecal community away from the Sham profile, and Sr partially restored it (Fig. 4A–E and Table S2). Romboutsia and Turicibacter decreased after OVX and increased after Sr, whereas Streptococcus and unidentified Lachnospiraceae changed in the opposite direction. Romboutsia also increased after other bone-protective interventions in OVX rats [27]. Turicibacter abundance correlates with bone mass in OVX mice [28] and with systemic BMD in postmenopausal women on estrogen therapy [29]. These genera may therefore mark, or contribute to, a bone-friendly microbiota. Streptococcus and Lachnospiraceae have been linked to inflammation and infection-associated bone resorption [30–34], and their reduction by Sr agrees with the lower IL-6 we observed. These are correlative, genus-level findings from 16S rRNA sequencing of fecal DNA; functional conclusions need metagenomic and gnotobiotic work.

Thirty-six fecal metabolites differed between OVX and OVX-Sr rats and were enriched in lipid pathways. Five Sr-responsive metabolites stood out: the oxylipins (±)11(12)-EET, 9(S)-HOTrE and 13(S)-HOTrE, and the PUFA-containing lipids 1-O-hexadecyl-lyso-sn-glycero-3-phosphocholine and PC(18:2/20:3). Oxylipins are short-lived signaling lipids produced from polyunsaturated fatty acids by lipoxygenase, cyclooxygenase and cytochrome P450 enzymes, and they act at the interface of diet, inflammation and tissue homeostasis. EET levels change with age in mouse bone marrow, muscle and serum [35], linking lipid mediators to musculoskeletal function. Fecal oxylipins reflect endogenous production, microbial metabolism and biliary/gut excretion, not systemic bioavailability. In the systemic compartment, EETs are generally bone-protective: they suppress osteoclastogenesis, support angiogenesis–osteogenesis coupling, and sEH inhibition, which raises EETs, reduces ovariectomy-induced bone loss in rodents [36, 37]. The higher fecal (±)11(12)-EET in OVX rats and its decline after Sr therefore do not show that EETs

harm bone. A better interpretation is that fecal EET/HOTrE levels track disturbed PUFA/epoxide metabolism in OVX, and that Sr partly normalizes this state. Fecal (±)11(12)-EET correlated with bone turnover markers and trabecular parameters (Fig. 6), supporting its use as a readout of metabolic status rather than a causal mediator. 9(S)-HOTrE and 13(S)-HOTrE are α-linolenic-acid-derived oxylipins linked to menopausal hot flushes [38]; their decline after Sr may reflect broader lipid improvement.

Enrichment pointed to linoleic acid metabolism and other lipid routes. LA (18:2n-6) is an essential dietary fatty acid, and its intake and circulating metabolites have been linked to bone mineral density in humans [39, 40]. The Sr-responsive metabolites here are not LA itself, but oxylipins and PUFA-containing lipids derived from LA, α-linolenic acid and arachidonic acid. The enrichment is therefore best explained by broader remodeling of PUFA/oxylipin metabolism rather than a specific LA effect. PUFA-derived lipids can act directly on skeletal cells: oleic and linoleic acids promote chondrocyte apoptosis via SIRT1/FOXO1-dependent autophagy inhibition [41], and linoleic acid impairs early MC3T3-E1 differentiation [42]. Excess n-6 PUFA is pro-inflammatory [43–45], and inflammation promotes bone resorption [46, 47]. The Sr-associated oxylipin shift, together with lower IL-6, may therefore influence the skeletal environment. Direct testing remains beyond this study.

Several Sr-responsive metabolites correlated with bone phenotypes across the three groups, and fecal (±)11(12)-EET showed the broadest correlations with biomechanical, microstructural and biochemical indices (Fig. 6). In pooled data (n = 18), (±)11(12)-EET was the metabolite most closely associated with bone turnover, microarchitecture and biomechanics (Fig. 6B–I). DEX is widely used to induce osteoblast injury and apoptosis in vitro [48]. Sr reversed DEX-suppressed proliferation, osteogenic-marker expression (ALP, BMP-2, BSP, CBF-α1, CT, OCN, P1NP and RUNX2) and matrix mineralization in MC3T3-E1 cells, confirming a direct, microbiota-independent pro-osteogenic effect. Together, the data indicate that dietary Sr acts directly on bone cells and also remodels the gut microbiota and fecal lipid metabolism, supporting a dual bone-cell and microbiota–metabolite route in PMOP protection.

This study has several limitations. First, Sr was given from the day of OVX (prevention design), so established bone loss was not modeled. Second, no Sham + Sr group was included, so effects in estrogen-replete animals are unknown. Third, the microbiota and metabolome analyses are descriptive and correlational; causality was not tested by fecal microbiota transplantation, microbiota depletion or metabolite rescue, and the group size (n = 6) limits power. Fourth, metabolites were measured in feces, not serum or bone, so their link to systemic or skeletal pools is unclear. Fifth, distal-femur BMD did not differ significantly between OVX and OVX-Sr rats, and benefits were captured mainly by trabecular parameters, histomorphometry and biomechanics. Finally, only one rodent model and one time point were studied, limiting translation to humans. These limitations define the next mechanistic questions; they do not alter the core finding that Sr improves the bone phenotype alongside microbiota–metabolite remodeling.

5. Conclusion

Dietary $SrCl_2$ reduced OVX-induced bone loss by suppressing pathological turnover, preserving trabecular microarchitecture and biomechanics, and lowering osteoclast numbers. It also directly promoted osteoblast differentiation and mineralization. These benefits were closely linked to gut microbiota and fecal oxylipin remodeling, and fecal (±)11(12)-EET correlated with bone turnover, microarchitecture and biomechanics. The findings identify a microbiota–oxylipin–bone axis in the skeletal response to Sr and support dietary $SrCl_2$ as a candidate bone-protective strategy for PMOP; a schematic summary is shown in Fig. 8.

Declarations

Ethics Approval:

Animal experiments were approved by the Committee on the Ethics of Animal Experiments, Chinese Academy of Agricultural Sciences (IAS2022-146), and complied with institutional guidelines.

Consent to Participate

Not applicable.

Consent for Publication

Not applicable.

Competing Interests

No competing interests were reported by the authors.

Funding

Funding was provided by the National Key R&D Program of China (2022YFD1301000), the CARS earmarked fund (CARS-36) and the Agricultural Science and Technology Innovation Program (ASTIP-IAS12).

Author Contribution

XXY, GYN, WJQ and ZN conceived the study; XXY and LXK conducted the experiments; XXY and YQQ wrote and revised the manuscript; ZN supervised the work and took primary responsibility for the final content. All authors approved the submitted version.

Acknowledgement

Not applicable.

Supplementary Information

Supplemental Figure S1–S4

Data Availability

The 16S rRNA sequencing and untargeted metabolomics data are provided in Supplemental Data S1–S6. Per-animal bone and serum phenotype values are available as Source Data. Raw sequencing and metabolomics files can be requested from the corresponding author.

References

1. Walker MD, Shane E Postmenopausal osteoporosis. The New England Journal of Medicine. 2023/11/23 2023;389(21):1979–1991
2. Eastell R, O'Neill TW, Hofbauer LC, Langdahl B, Reid IR, Gold DT et al (2016) Postmenopausal osteoporosis. Nat Reviews Disease Primers 2(1):16069
3. Liu Z, Xu X, Shen Y, Hao Y, Cui W, Li W et al (2022) Altered gut microbiota and metabolites profile are associated with reduced bone metabolism in ethanol-induced osteoporosis. Cell Prolif Jul 55(7):e13245 Epub 2022/06/11
4. He LY, Sun Y, Yao WJ et al (2016) Prevalence of osteoporosis in Chinese elderly aged 60 years and older from 2010 to 2016: a meta-analysis [in Chinese]. Chin J Osteoporos 2016/12/01 22(12):1590–1596
5. Ni X, Wu B, Li S, Zhu W, Xu Z, Zhang G et al (2023) Equol exerts a protective effect on postmenopausal osteoporosis by upregulating OPG/RANKL pathway. Phytomedicine 108:154509
6. Zhou Y, Deng Y, Liu Z, Yin M, Hou M, Zhao Z et al (2021) Cytokine-scavenging nanodecoys reconstruct osteoclast/osteoblast balance toward the treatment of postmenopausal osteoporosis. Sci Adv 7(48):eabl6432
7. Ding K, Hua F, Ding W (2020) Gut Microbiome and Osteoporosis. Aging Disease 11(2):438
8. Behera J, Ison J, Tyagi SC, Tyagi N (2020) The role of gut microbiota in bone homeostasis. Bone 135:115317
9. Shi N, Li N, Duan X, Niu H (2017) Interaction between the gut microbiome and mucosal immune system. Military Med Res 4(1):14
10. Ohlsson C, Sjögren K (2015) Effects of the gut microbiota on bone mass. Trends Endocrinol Metabolism 26(2):69–74
11. Villa CR, Ward WE, Comelli EM (2015) Gut microbiota-bone axis. Crit Rev Food Sci Nutr 57(8):1664–1672

12. Yan J, Takakura A, Zandi-Nejad K, Charles JF (2017) Mechanisms of gut microbiota-mediated bone remodeling. Gut Microbes 9(1):84–92
13. Chen Y, Yang C, Dai Q, Tan J, Dou C, Luo F (2023) Gold-nanosphere mitigates osteoporosis through regulating TMAO metabolism in a gut microbiota-dependent manner. J Nanobiotechnol 21(1):125
14. Li J-Y, Chassaing B, Tyagi AM, Vaccaro C, Luo T, Adams J et al (2016) Sex steroid deficiency-associated bone loss is microbiota dependent and prevented by probiotics. J Clin Investig 126(6):2049–2063
15. Zhang Y-W, Cao M-M, Li Y-J, Lu P-P, Dai G-C, Zhang M et al (2022) Fecal microbiota transplantation ameliorates bone loss in mice with ovariectomy-induced osteoporosis via modulating gut microbiota and metabolic function. J Orthop Translation 37:46–60
16. Pors Nielsen S (2004) The biological role of strontium. Bone 35(3):583–588
17. Ru X, Yang L, Shen G, Wang K, Xu Z, Bian W, Zhu W, Guo Y (2024) Microelement strontium and human health: comprehensive analysis of the role in inflammation and non-communicable diseases (NCDs). Front Chem 12:1367395
18. Tomczyk-Warunek A, Turzanska K, Posturzynska A, Kowal F, Blicharski T, Pano IT, Winiarska-Mieczan A, Nikodem A, Dresler S, Sowa I, Wojciak M, Dobrowolski P (2024) Influence of various strontium formulations (ranelate, citrate, and chloride) on bone mineral density, morphology, and microarchitecture: a comparative study in an ovariectomized female mouse model of osteoporosis. Int J Mol Sci 25(7):4075
19. Bonnelye E, Chabadel A, Saltel F, Jurdic P (2008) Dual effect of strontium ranelate: stimulation of osteoblast differentiation and inhibition of osteoclast formation and resorption in vitro. Bone 2008/01/01 42(1):129–138
20. Ammann P, Shen V, Robin B, Mauras Y, Bonjour JP, Rizzoli R (2004) Strontium ranelate improves bone resistance by increasing bone mass and improving architecture in intact female rats. Journal of Bone and Mineral Research. /12/01 2004;19(12):2012–2020
21. Xi X, Gao Y, Wang J, Zheng N (2023) Strontium chloride improves bone mass by affecting the gut microbiota in young male rats. Front Endocrinol 14:1198475
22. Peng S, Liu XS, Huang S, Li Z, Pan H, Zhen W et al (2011) The cross-talk between osteoclasts and osteoblasts in response to strontium treatment: Involvement of osteoprotegerin. Bone 49(6):1290–1298
23. Li Y, Li J, Zhu S, Luo E, Feng G, Chen Q et al (2012) Effects of strontium on proliferation and differentiation of rat bone marrow mesenchymal stem cells. Biochem Biophys Res Commun 418(4):725–730
24. Zhu S, Hu X, Tao Y, Ping Z, Wang L, Shi J et al (2016) Strontium inhibits titanium particle-induced osteoclast activation and chronic inflammation via suppression of NF-κB pathway. Sci Rep 6(1):36251
25. Eastell R, Szulc P (2017) Use of bone turnover markers in postmenopausal osteoporosis. Lancet Diabetes Endocrinol 5(11):908–923

26. Peng H, Yao F, Xiong S, Wu Z, Niu G, Lu T (2021) Strontium in public drinking water and associated public health risks in Chinese cities. Environ Sci Pollut Res 28(18):23048–23059
27. Song C, Ma Y, Wang Y, Li P, Chen Y, Liu H et al (2023) Diosgenin reduces bone loss through the regulation of gut microbiota in ovariectomized rats. Gene 869:147383
28. Wan X, Eguchi A, Fujita Y, Ma L, Wang X, Yang Y et al (2022) Effects of (R)-ketamine on reduced bone mineral density in ovariectomized mice: A role of gut microbiota. Neuropharmacology 213:109139
29. Lecomte M, Tomassi D, Rizzoli R, Tenon M, Berton T, Harney S et al (2023) Effect of a Hop Extract Standardized in 8-Prenylnaringenin on Bone Health and Gut Microbiome in Postmenopausal Women with Osteopenia: A One-Year Randomized, Double-Blind, Placebo-Controlled Trial. Nutrients 15(12):2688
30. Johani K, Fritz BG, Bjarnsholt T, Lipsky BA, Jensen SO, Yang M et al (2018) Understanding the microbiome of diabetic foot osteomyelitis: insights from molecular and microscopic approaches. Clin Microbiol Infect 24(6):660–667
31. Fan Z, Pathak JL, Ge L (2021) The potential role of RP105 in regulation of inflammation and osteoclastogenesis during inflammatory diseases. Front Cell Dev Biology 9:713254
32. Zhao B, Grimes SN, Li S, Hu X, Ivashkiv LB (2012) TNF-induced osteoclastogenesis and inflammatory bone resorption are inhibited by transcription factor RBP-J. J Exp Med 209(2):319–334
33. Cosme-Silva L, Dal-Fabbro R, Cintra LTA, Ervolino E, Prado ASAd O, DPd et al (2021) Dietary supplementation with multi-strain formula of probiotics modulates inflammatory and immunological markers in apical periodontitis. J Appl Oral Sci 29:e20210483
34. Zeng H, Ishaq SL, Zhao F-Q, Wright A-DG (2016) Colonic inflammation accompanies an increase of β-catenin signaling and Lachnospiraceae/Streptococcaceae bacteria in the hind gut of high-fat diet-fed mice. J Nutr Biochem 35:30–36
35. Al Saedi A, Wang Z, Shah A, Brotto M, Duque G (2022) Comparative analysis of fat composition in marrow, serum, and muscle from aging C57BL6 mice. Mech Ageing Dev 206:111690
36. Guan H, Zhao L, Cao H, Chen A, Xiao J (2015) Epoxyeicosanoids suppress osteoclastogenesis and prevent ovariectomy-induced bone loss. The FASEB Journal. /03/01 2015;29(3):1092–1101
37. Gao L et al (2023) Targeting soluble epoxide hydrolase promotes osteogenic-angiogenic coupling via activating SLIT3/HIF-1α signalling pathway. Cell Proliferation. /07/01 2023;56(7):e13403
38. Martinez JA, Wertheim BC, Roe DJ, Taljanovic MS, Chow HHS, Chew W et al (2023) Oxylipins as Biomarkers for Aromatase Inhibitor-Induced Arthralgia (AIA) in Breast Cancer Patients. Metabolites 13(3):452
39. Ros E (2020) Linoleic acid intake and reduction in mortality: the icing on the cake of health benefits from n-6 PUFAs? Am J Clin Nutr 112(1):3–4
40. Bellissimo MP, Ziegler TR, Jones DP, Liu KH, Fernandes J, Roberts JL et al (2021) Plasma High-Resolution Metabolomics Identifies Linoleic Acid and Linked Metabolic Pathways Associated with Bone Mineral Density. Clin Nutr 40(2):467–475

41. Xiaodong L, Chen Z, Chuanyuan M, Guantong S, Fei Y, Lei W et al (2024) Oleic and linoleic acids promote chondrocyte apoptosis by inhibiting autophagy via downregulation of SIRT1/FOXO1 signaling. Biochimica et Biophysica Acta (BBA) -. Mol Basis Disease 1870(4):167090
42. Paula-Dene N, Thomas Z, Daiana W, Li H, Matthew S, Dean J et al (2022) Linoleic Acid Reduces Oxidative Phosphorylation and Impairs Early Differentiation of MC3T3-E1 Osteoblast Precursor Cells. Curr Developments Nutr 6:452
43. Du J, Chen Q, Li Y, Xiang X, Xu W, Mai K et al (2020) Activation of the Farnesoid X Receptor (FXR) Suppresses Linoleic Acid-Induced Inflammation in the Large Yellow Croaker (Larimichthys crocea). J Nutr 150(9):2469–2477
44. Yang B, Ji R, Li X, Fang W, Chen Q, Chen Q et al (2021) Activation of Autophagy Relieves Linoleic Acid-Induced Inflammation in Large Yellow Croaker (Larimichthys crocea). Front Immunol 12:649385
45. Cao JJ, Gregoire BR, Michelsen KG, Picklo MJ (2020) Decreasing the Ratio of Dietary Linoleic to α-Linolenic Acid from 10 to 4 by Changing Only the Former Does Not Prevent Adiposity or Bone Deterioration in Obese Mice. J Nutr 150(6):1370–1378
46. Rao S-S, Hu Y, Xie P-L, Cao J, Wang Z-X, Liu J-H et al (2018) Omentin-1 prevents inflammation-induced osteoporosis by downregulating the pro-inflammatory cytokines. Bone Res 6(1):9
47. Adami G (2022) Regulation of bone mass in inflammatory diseases. Best Pract Res Clin Endocrinol Metab 36(2):101611
48. Rai R, Singh KB, Khanka S, Maurya R, Singh D (2022) Cladrin alleviates dexamethasone-induced apoptosis of osteoblasts and promotes bone formation through autophagy induction via AMPK/mTOR signaling. Free Radic Biol Med 190:339–350

Figures

Figure1

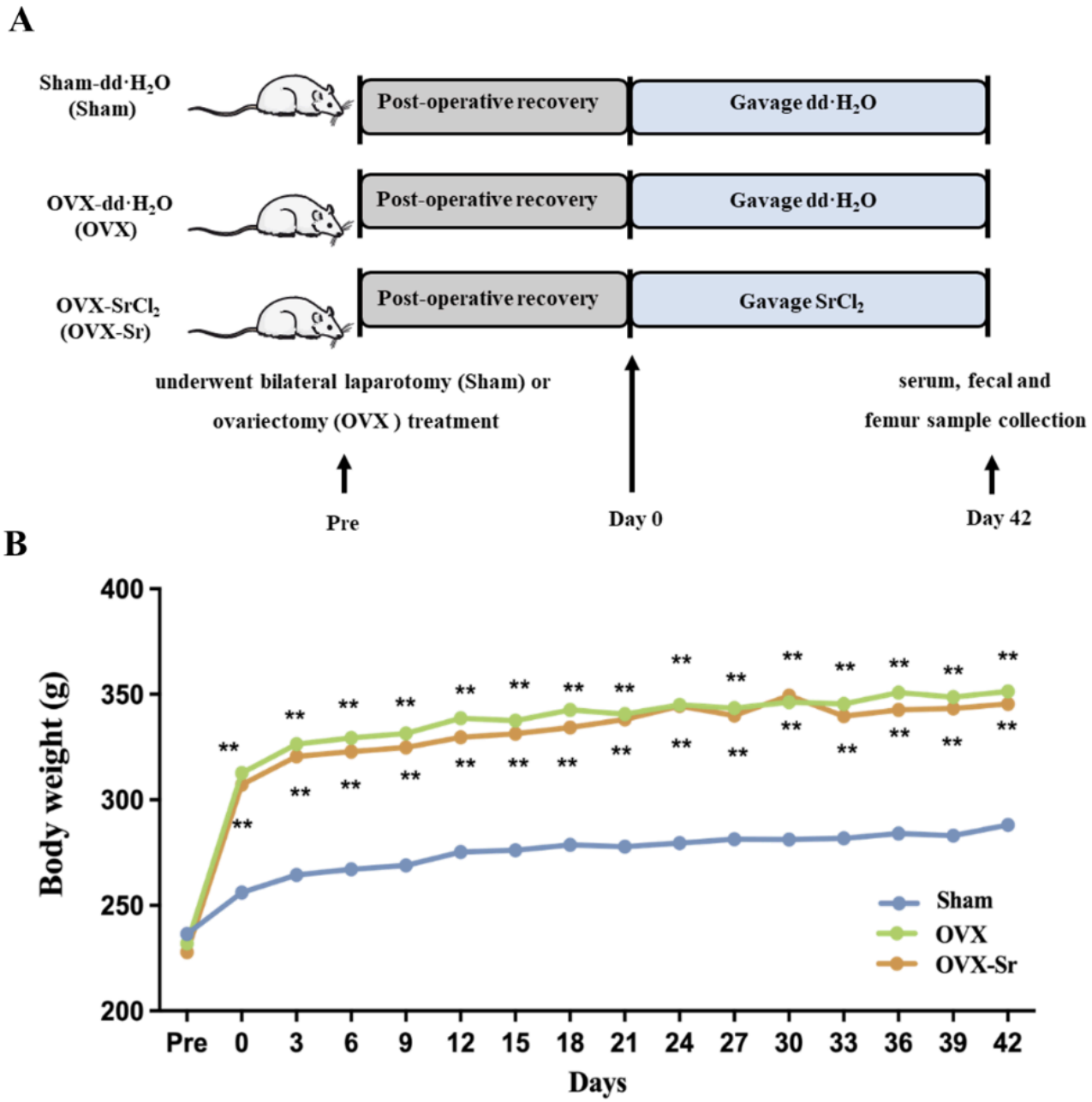


Figure 1

Experimental workflow and effects of Sr on growth. (A) Study timeline and group allocation. (B) Average body weight. Values are mean ± SD (n = 6). Significance was assessed by one-way ANOVA with Tukey's post hoc test: *P < 0.05, **P < 0.01 versus Sham.

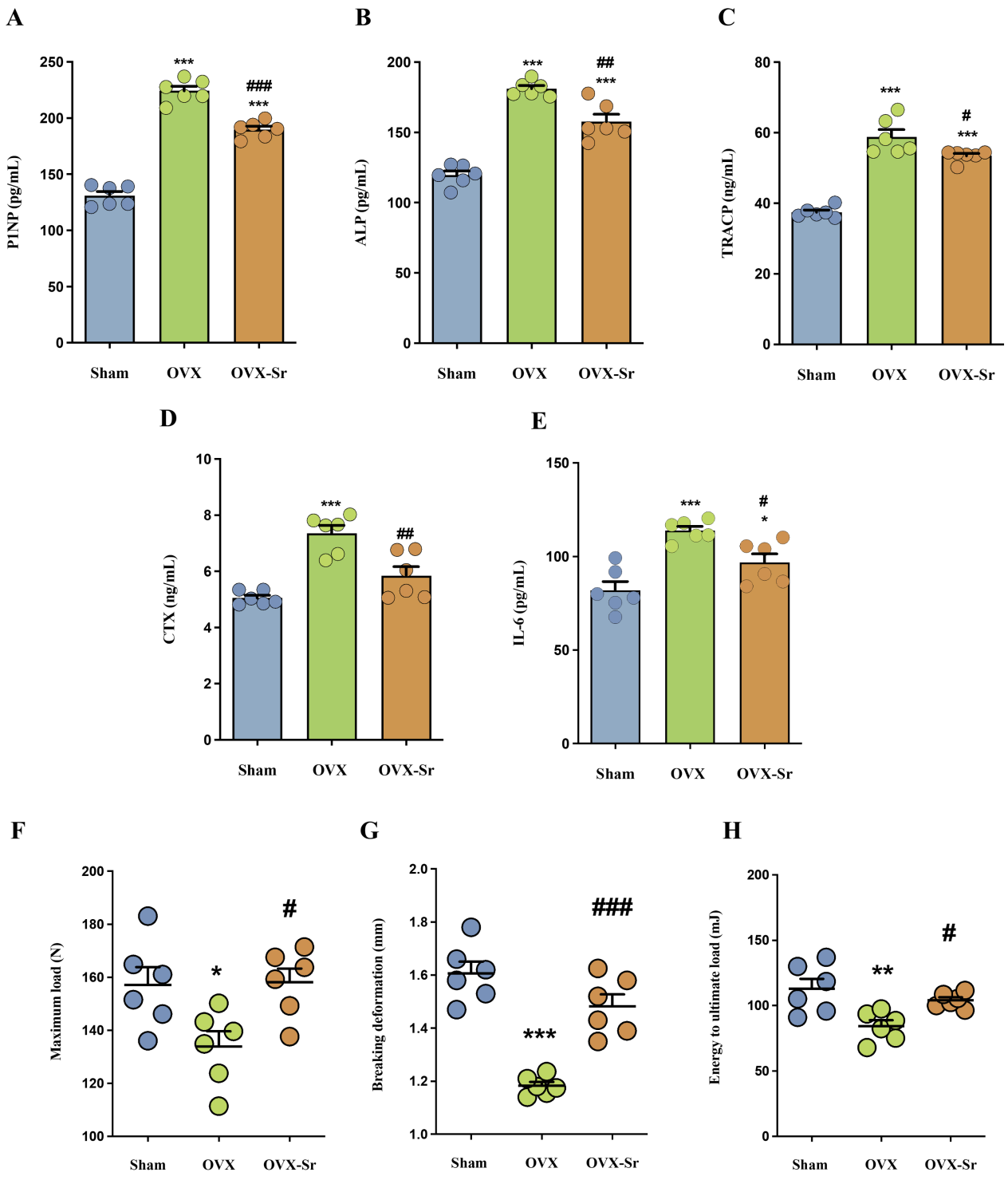


Figure 2

Effects of Sr on bone turnover and biomechanics. Serum levels of (A) P1NP, (B) ALP, (C) TRACP, (D) CTX and (E) IL-6. (F) Maximum load, (G) breaking deformation and (H) energy to ultimate load (n = 6). Data are mean ± SD. Significance: *P < 0.05, **P < 0.01, ***P < 0.001 versus Sham; #P < 0.05, ##P < 0.01, ###P < 0.001 versus OVX.

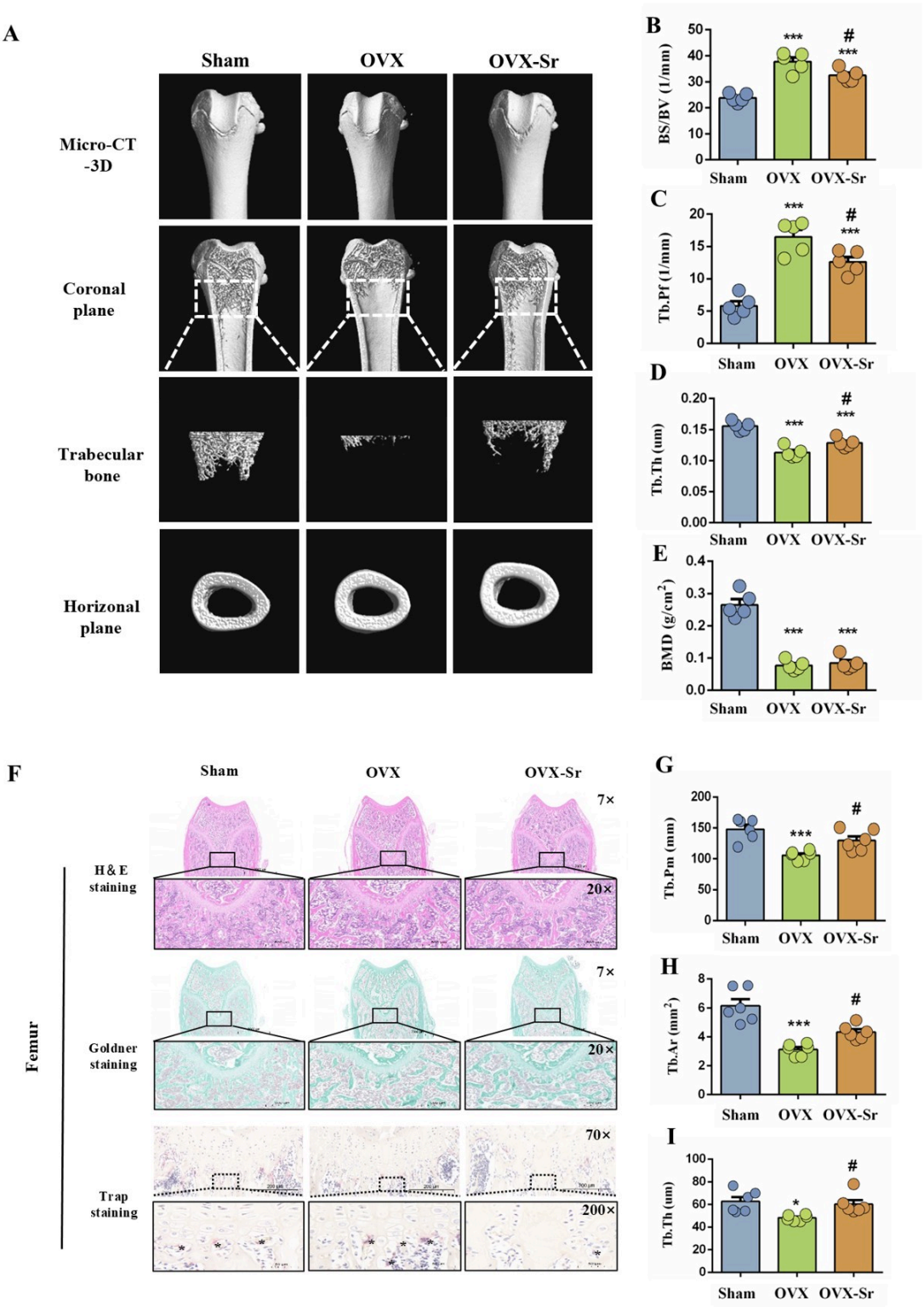


Figure 3

Effects of Sr on bone microarchitecture and morphology. (A) Representative micro-CT images of the femur. (B–E) Trabecular BS/BV, Tb.Pf, Tb.Th and BMD (n = 5). (F) H&E, Goldner (7× and 20×) and TRAP (70× and 200×) staining; scale bar, 200 μm. (G–I) Tb.Pm, Tb.Ar and Tb.Th (n = 6). Data are mean ± SD. *P < 0.05 and ***P < 0.001 versus Sham; #P < 0.05 versus OVX.

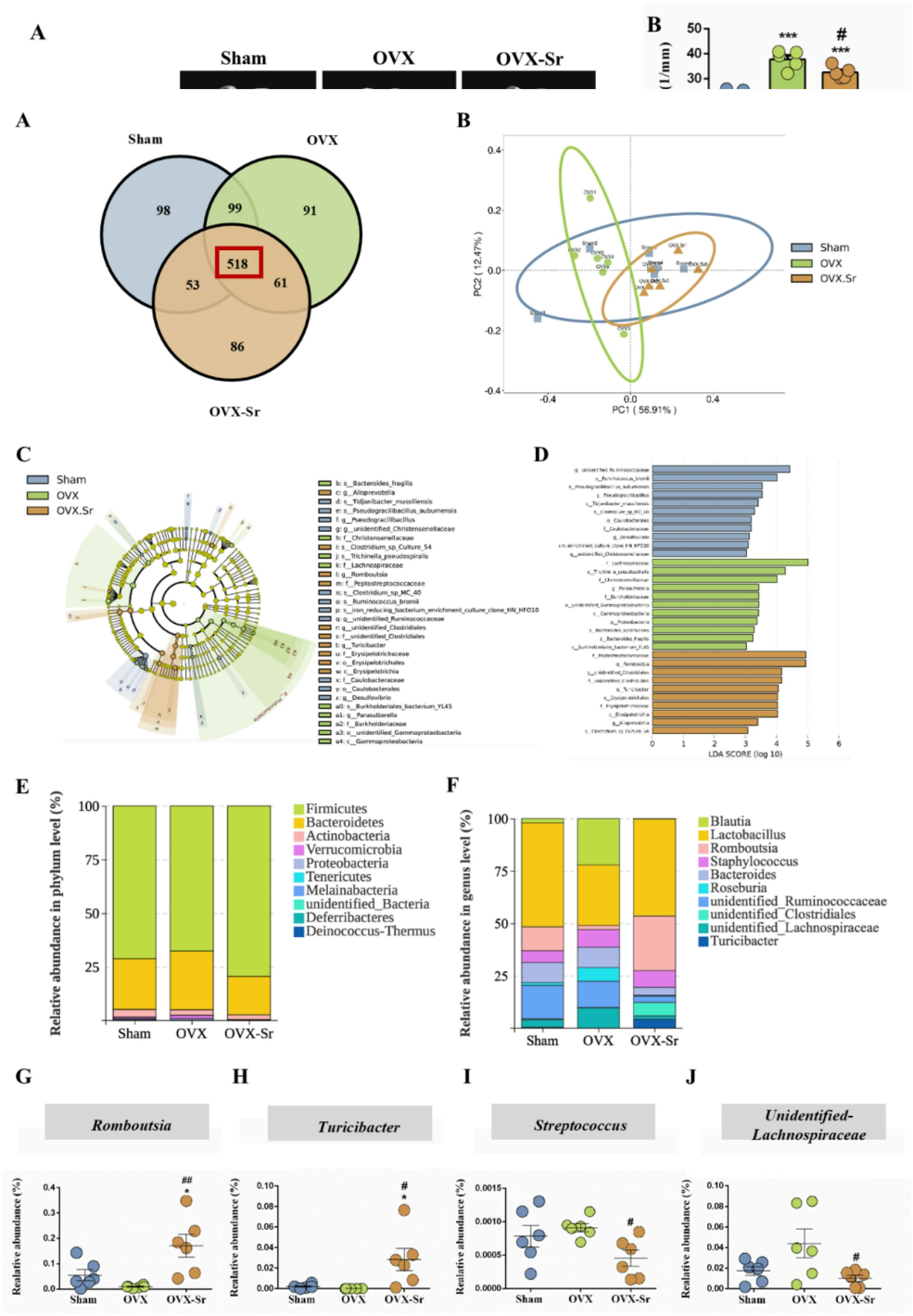


Figure 4

Effects of Sr on gut microbiota structure. (A) Venn diagram. (B) PCA based on unweighted UniFrac distances. (C) LEfSe cladogram. (D) LDA scores. Relative abundance at phylum (E) and genus (F) levels. (G–J) Romboutsia, Turicibacter, Streptococcus and unidentified Lachnospiraceae (n = 6). Data are mean ± SD. *P < 0.05 versus Sham; #P < 0.05 versus OVX.

Figure5

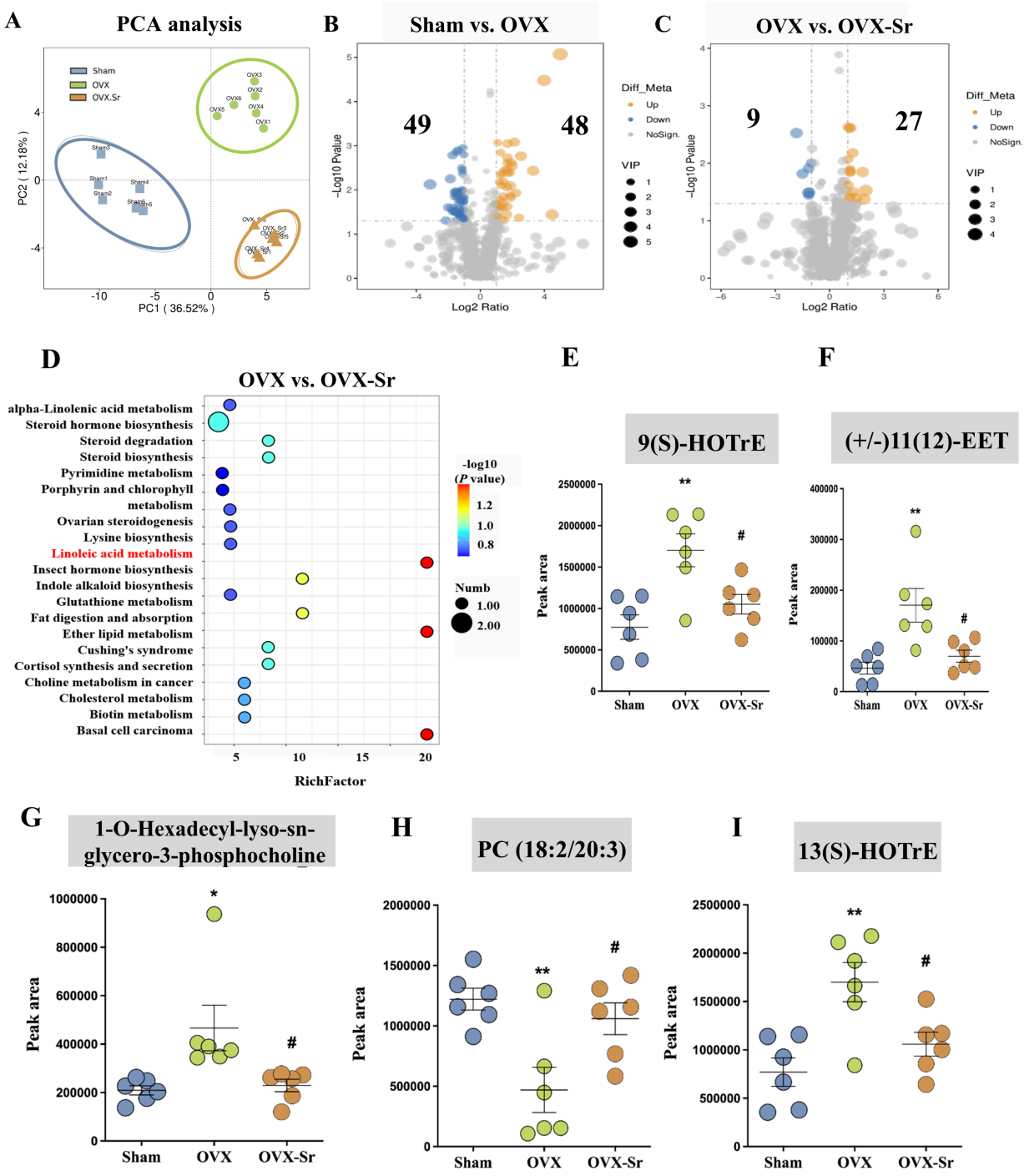


Figure 5

Effects of Sr on the fecal metabolome. (A) PCA. Volcano plots for (B) Sham versus OVX, (C) Sham versus OVX-Sr and (D) OVX versus OVX-Sr. (E) Pathway enrichment for OVX versus OVX-Sr. Concentrations of (F) (±)11(12)-EET, (G) 9(S)-HOTrE, (H) 13(S)-HOTrE, (I) 1-O-hexadecyl-lyso-sn-glycero-3-phosphocholine and (J) PC(18:2/20:3) (n = 6). Data are mean ± SD. *P < 0.05 and **P < 0.01 versus Sham; #P < 0.05 versus OVX.

Figure6

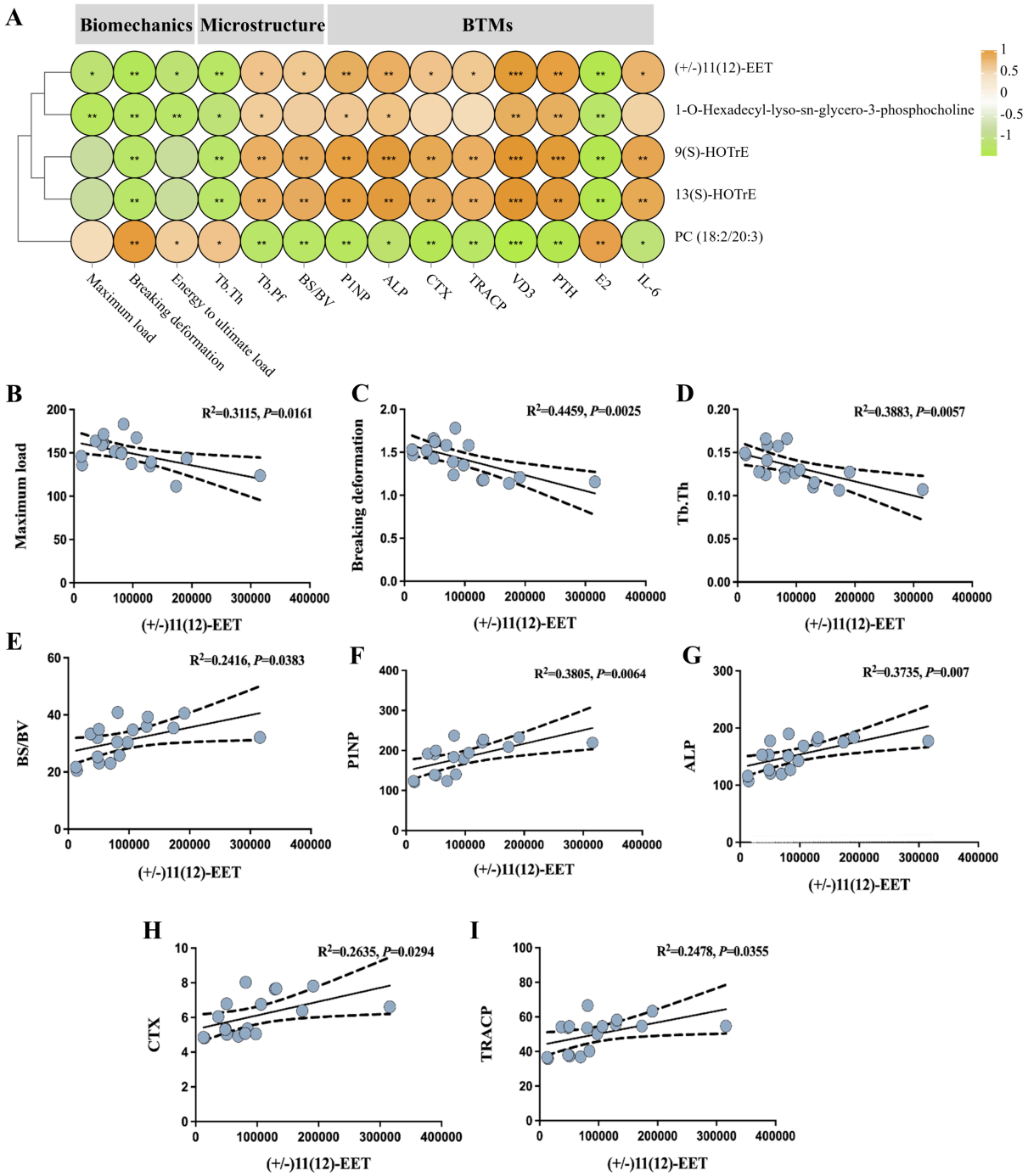


Figure 6

Integrated metabolome–phenotype analysis. (A) Pearson correlations between the five Sr-responsive metabolites and bone phenotypes. (B–I) Linear regressions of fecal (±)11(12)-EET against (B) maximum load, (C) breaking deformation, (D) Tb.Th, (E) BS/BV, (F) P1NP, (G) ALP, (H) CTX and (I) TRACP. Analyses used pooled data from all groups (n = 18). Significance: *P < 0.05, **P < 0.01, ***P < 0.001.

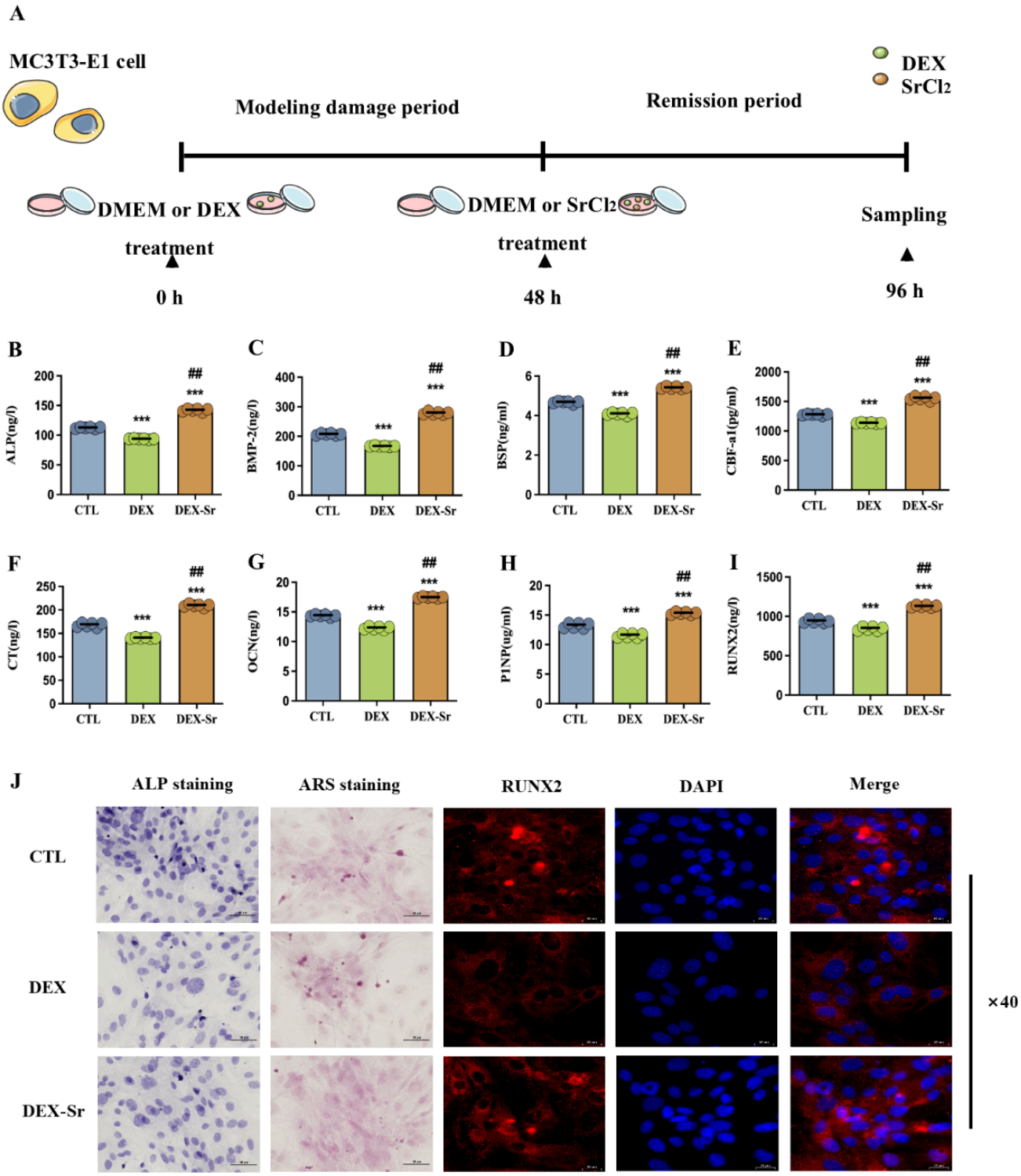


Figure 7

Effects of Sr on MC3T3-E1 cells. (A) Study timeline and group allocation. (B–I) Levels of ALP, BMP-2, BSP, CBF-α1, CT, OCN, P1NP and RUNX2 (n = 6). (J) ALP, ARS and RUNX2 immunofluorescence images (40×); scale bar, 50 μm. Data are mean ± SD from at least three independent experiments. ***P < 0.001 versus CTL; ##P < 0.01 versus DEX.

Figure8

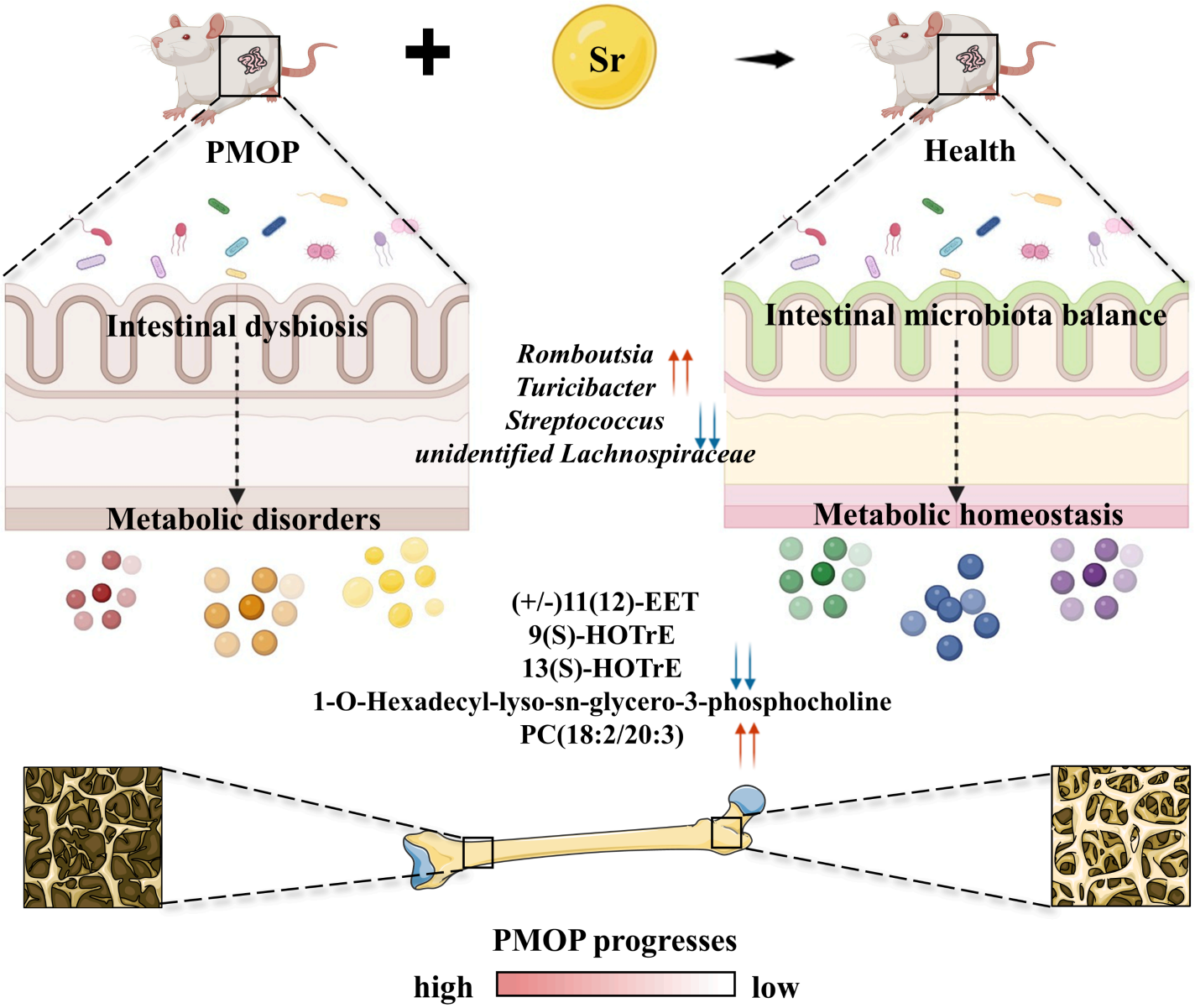


Figure 8

Schematic summary of the skeletal and gut-related effects of dietary strontium chloride in ovariectomized rats. Sr supplementation improved bone turnover markers, trabecular microstructure and femoral biomechanics. It also promoted osteoblast differentiation and mineralization *in vitro*. These effects were accompanied by remodeling of the gut microbiota and fecal lipid (oxylipin) metabolites, which correlated with bone phenotypes. Dashed arrows denote associations observed in this study; causality of the microbiota–metabolite–bone links remains to be established.

Supplementary Files

This is a list of supplementary files associated with this preprint. Click to download.

- Supplementaldata13.xlsx
- Supplementalinformation.docx